

Article

A Group Handover Scheme for Supporting Drone Services in IoT-Based 5G Network Architectures

Emmanouil Skondras¹, Ioannis Kosmopoulos¹, Emmanouel T. Michailidis^{2,*}, Angelos Michalas³ and Dimitrios D. Vergados¹

¹ Department of Informatics, University of Piraeus, 80 Karaoli and Dimitriou St., 18534 Piraeus, Greece

² Department of Information and Communication Systems Engineering, School of Engineering, University of the Aegean, 83200 Samos, Greece

³ Department of Electrical and Computer Engineering, University of Western Macedonia, Karamanli and Ligeris, 50131 Kozani, Greece

* Correspondence: emichail@aegean.gr

Abstract: Next generation mobile networks are expected to integrate multiple drones organized in Flying Ad Hoc Networks (FANETs) to support demanding and diverse services. The highly mobile drones should always be connected to the network in order to satisfy the strict requirements of upcoming applications. As the number of drones increases, they burden the network with the management of signaling and continuous monitoring of the drones during data transmission. Therefore, designing transmission mechanisms for fifth-generation (5G) drone-aided networks and using clustering algorithms for their grouping is of paramount importance. In this paper, a clustering and selection algorithm of the cluster head is proposed together with an efficient Group Handover (GHO) scheme that details how the respective Point of Access (PoA) groups will be clustered. Subsequently, for each cluster, the PoA elects a Cluster Head (CH), which is responsible for manipulating the mobility of the cluster by orchestrating the handover initiation (HO initiation), the network selection, and the handover execution (HO execution) processes. Moreover, the members of the cluster are informed about the impending HO from the CH. As a result, they establish new uplink and downlink communication channels to exchange data packets. In order to evaluate the proposed HO scheme, extensive simulations are carried out for a next-generation drone network architecture that supports Internet of Things (IoT) and multimedia services. This architecture relies on IEEE 802.11p Wireless Access for Vehicular Environment (WAVE) Road Side Units (RSUs) as well as Long-Term Evolution Advanced (LTE-A) and IEEE 802.16 Worldwide Interoperability for Microwave Access (WiMAX). Furthermore, the proposed scheme is also evaluated in a real-world scenario using a testbed deployed in a controlled laboratory environment. Both simulation and real-world experimental results verify that the proposed scheme outperforms existing HO algorithms.

Keywords: drone-to-drone (D2D) communication; drone-to-infrastructure (D2I) communication; flying ad hoc networks (FANET); group handover; mobility management



Citation: Skondras, E.; Kosmopoulos, I.; Michailidis, E.T.; Michalas, A.; Vergados, D.D. A Group Handover Scheme for Supporting Drone Services in IoT-Based 5G Network Architectures. *Drones* **2022**, *6*, 425. <https://doi.org/10.3390/drones6120425>

Academic Editors: Iván Vidal and Francisco Valera

Received: 22 November 2022

Accepted: 14 December 2022

Published: 17 December 2022

Publisher's Note: MDPI stays neutral with regard to jurisdictional claims in published maps and institutional affiliations.



Copyright: © 2022 by the authors. Licensee MDPI, Basel, Switzerland. This article is an open access article distributed under the terms and conditions of the Creative Commons Attribution (CC BY) license (<https://creativecommons.org/licenses/by/4.0/>).

1. Introduction

In recent years, the use of swarms of drones and Flying Ad Hoc Networks (FANETs) [1] has been proposed to enhance the connectivity of fifth generation (5G) communication networks, Internet of Things (IoT) [2,3], and Internet of Drones (IoD) [4]. The FANETs involve highly dynamic network deployments [5] with multiple interconnected drones configured in groups. In FANETs, each drone can support several services including disaster management applications [6], eHealth applications [7], and streaming of multimedia content [8]. Drones can be equipped with Onboard Units (OBUs) [9,10] with computational, storage, and communication resources. In addition, some OBUs integrate IoT devices (e.g., speedometers and acceleration sensors) [11]. Moreover, Drone-to-Drone (D2D) [12] and Drone-to-Infrastructure (D2I) [13] communication can be established by leveraging

Wireless Access in the Vehicular Environment (WAVE) Road Side Units (RSUs) [14,15], Long-Term Evolution Advanced (LTE-A) eNodeBs [16–18], and IEEE 802.16 Worldwide Interoperability for Microwave Access (WiMAX) Base Stations (BSs) [19,20].

In the special case of FANETs, a set of drones may simultaneously perform a handover (HO) to a new Point of Access (PoA). In addition, Group HOs (GHOs) may occur in cases where multiple drones with similar trajectories move from the coverage area of a PoA to the coverage area of another PoA. Among the advantages of GHOs is the reduction of the signaling burden on the network by simultaneously handing over multiple drones to the new PoA. As long as each drone carries out the HO individually, the required signaling is increased.

In order to perform a GHO, clustering of drones is deemed necessary. A clustered infrastructure consists of groups of drones called clusters, where the drones of each cluster have similar characteristics, such as speed, movement direction, received signal strength, or Quality of Service (QoS). In addition, the two main components of a cluster are the Cluster Head (CH) and the Cluster Member (CM). Typically, there is one main node for each cluster, i.e., the CH, which provides management services, such as media access, packet and message routing, optimal path-finding for long-distance packets, bandwidth allocation, and packet transmission within the cluster. Each CH can communicate with the CMs of its cluster, while in some cases, communication between CHs of different clusters can be performed. On the other hand, a CM is a simple member of a cluster [21].

Although clustering is typically used to solve mobility management, data routing, or resource allocation issues, existing algorithms from Mobile Ad Hoc Networks (MANETs) cannot successfully handle mobility problems arising from complex and highly dynamic FANET deployments. As a result, existing algorithms should be enhanced to support cluster of drones instead of supporting only individual mobile equipment. However, the time interval of cluster creation and maintenance adds additional overhead to the network owing to the complex nature of FANETs [22].

Motivated by the aforementioned observations, this paper proposes a GHO framework. The major contributions of this paper are synopsized as follows:

- A scheme that enables the creation of clusters of drones is introduced, including an algorithm for the election of a CH for each cluster.
- A Group HO methodology is implemented, including HO initiation, network selection, and HO execution processes, resulting in the minimization of the HO signaling costs.
- During the HO initiation, decision making is performed by taking into consideration the relative importance between multiple services including IoT and multimedia drone applications.
- The creation of a candidate networks list and the ranking of network alternatives are performed at the fog and cloud infrastructures in order to minimize the workloads at each drone.

The remainder of this paper is organized as follows: In Section 2, the related research literature is summarized. In addition, in Section 3, the proposed GHO scheme is described. Section 4 presents the simulation setup and the simulation results, while Section 5 evaluates the proposed scheme in real-world scenarios using an experimental testbed. Finally, Section 6 provides concluding remarks and discusses future research perspectives.

2. Background

In recent years, several HO management schemes for drone-aided network architectures have been proposed. Indicatively, as described in [23], among the main challenges in such network infrastructures is the provision of seamless network connectivity to drones, the handling of the increased mobility of drones, the design and development of efficient network selection algorithms, the manipulation of HO failures, and the minimization of the ping-pong effects that may occur during an HO. Furthermore, some authors have proposed methodologies for performing GHOs in order to minimize the HO signaling cost. In this section, some indicative works are discussed.

2.1. HO/GHO Schemes for Drone-Aided Networks

To address the issue of mobility management in drone networks, the Cluster-Based Routing for Sparse and Dense Networks (CBRSDN) algorithm was proposed in [24], as a comprehensive solution for creating clusters in drone-aided networks, selecting the CH of each cluster, and managing it smoothly. More specifically, a process was described, where the drones were divided into clusters with common characteristics, and one of these drones exchanged data with all network entities. This protocol was responsible for establishing a route between the source and destination of information when an arbitrary node intended to send packets to a destination. The specific algorithm was parameterized to appropriately adapt to several transmission scenarios.

Furthermore, in [25], a GHO scheme was proposed to increase capacity by deploying Drone Base Stations (DBSs). It was considered that a large amount of User Equipment (UE) can decrease the QoS and lead to service interruption. Particularly, the proposed scheme benefited from the GHO by electing the serving PoA as a group manager and resolved security issues concerning the authentication of nodes. The UE was handled at the DBS as a group, whereas data transmission between PoAs was not assessed. Moreover, the authentication process included two parts. Firstly, the DBSs were authenticated from the serving PoA using public keys. Then, the UE was authenticated by the DBSs, and the total HO time and energy consumption were decreased.

In [26], a machine learning (ML) HO mechanism was proposed to provide seamless connectivity for drone user equipment in a cellular environment. In this approach, the mechanism that enabled the connection to the cell with the highest Reference Signal Received Power (RSRP) was inadequate owing to the speed and flight trajectory of the drone. Thus, a Reinforcement Learning (RL)-based Q-learning algorithm was presented that considered a weighted function and included the values of the HO cost and the serving cell RSRP. This algorithm took into account the current state of the drone and the future state as a reward, which was estimated with a weighted function. The experimental results demonstrated that the proposed algorithm outperforms the standard RSRP cell selection algorithm by reducing the ping-pong effects and the signaling overhead. Additionally, this algorithm decreases the overall number of HOs during a flight, while connecting to the strongest cell at the same time.

2.2. HO Schemes for Other Network Infrastructures

Previously, several schemes that perform HO operations without performing mobility management in drone-aided networks have also been proposed. As such schemes describe fully functional HO methodologies, they can be applied to drone network infrastructures, maybe with modifications in some cases.

Indicatively, in [27], a mobility management model for LTE networks was presented with support of both macrocells and femtocells. In particular, a load-aware algorithm was described, which determined two HO thresholds, namely the γ_{th}^M and the γ_{th}^F , for macrocells and femtocells, respectively. These thresholds were calculated considering both the simple Reference Signal Received Power (RSRP)-based threshold defined in LTE as well as the network load information. When the RSRP dropped below the corresponding γ_{th} threshold, a Time-to-Trigger (TTT) timer was initialized to a certain value T , considering various parameters, such as the cell transmission power, the distances between the available cells, the path loss, the carrier frequency, the network traffic load, and the user velocity. During the countdown, the timer stops, and the user remains in the current network, provided that the RSRP returns above the corresponding γ_{th} threshold. In addition, the user should perform an HO to the network with the highest RSRP as soon as the timer equals zero. It is noted that this scheme can easily be applied to a drone network infrastructure, where the drones act as users.

In [28], a radio access selection algorithm for vehicular environments was proposed. The authors defined two network interface types, namely the primary interface and the secondary interface. In addition, the 802.11p network access technology was considered

as the primary interface, while the 3GPP LTE was considered as the secondary one. By default, the vehicle was connected to the primary interface. The HO was initiated when the observed packet loss of user applications exceeded a maximum acceptable threshold. In this case, the vehicle performed an HO to the secondary interface. Thereafter, a timer was considered that specified the time duration when the secondary interface was used. As soon as the timer expired, the offered packet loss ratio of the primary interface was checked. Moreover, the vehicle performed an HO back to the primary interface when the packet loss ratio, which was offered by the primary interface, became lower than the maximum acceptable threshold. Although vehicular environments with ground nodes were considered, the proposed scheme can also be modified to include aerial ones.

In [29], a two-phase HO management scheme was proposed. Initially, the simple Received Signal Strength (RSS) -based HO initiation mechanism was applied, where the HO initiation took place when the observed RSS became lower than a predefined RSS threshold. Then, during the second phase, a triangular fuzzy Multi-Attribute Decision Making (MADM) algorithm was used that considered parameters, such as the RSS, the delay, the network load, and the battery utilization. This scheme can be applied to several types of network infrastructures, including drone-aided networks, since the aforementioned parameters can be available regardless of the type of the implemented network.

In [30], an IoT-enabled and Secrecy Aware GHO scheme (ISAG) for e-health services was introduced. The ISAG was applied to a Machine-to-Machine (M2M) communication network, where M2M devices (MMDs) provided services for patients. Specifically, the data transmission in the aforementioned scenario required both reliability and integrity, which were not fulfilled using standard HO algorithms. In this direction, several techniques were adopted to handle security issues during data transmission. The proposed scheme improved the HO preparation and registration processes by electing group leaders who aggregated the message authentication of the HO process. Notably, the group leader transmitted the aggregated request and response messages to the Home Subscriber Server (HSS) and the MMDs respectively. Hence, the computation, transmission, storage, and communication costs were decreased. The aforementioned scheme may also be applied to drone-aided networks, with D2D communication links.

3. The Proposed GHO Scheme for Drone-Aided Networks

In this section, a GHO scheme called enhanced-CBRSDN (eCBRSND) is proposed that improves the CBRSDN algorithm, which as presented in [24] performs better than alternative solutions in both cluster formation and CH election procedures. The implementation of the procedures of this algorithm are also presented, including the clustering, the election of a CH for each cluster, and the handling of the mobility issues of the drones.

3.1. The Design of the Proposed Scheme

Figure 1 depicts the three-layer design of the proposed GHO scheme that consists of the Drone Layer (DL), the Access Network Layer (ANL), and the Service Layer (SL). The DL includes multiple drones, the ANL includes a set of PoAs, and the SL deploys a number of drone services. Each PoA of the ANL provides network access to a subset of the drones, which is organized into clusters, in order to efficiently handle their increased mobility. In addition, through the aforementioned network access, each drone obtains access to the services of the SL. Note that the SL can be implemented either on a Cloud infrastructure or on several physical servers.

3.2. The Clustering Process

The clustering process constitutes a key factor for efficient drone separation, whereas the goal of the proposed scheme is network load balancing and optimized bandwidth utilization. It is considered that the drones and PoAs are aware of their geographic location within the area covered by the access network. Moreover, each PoA is informed about the position of each drone.

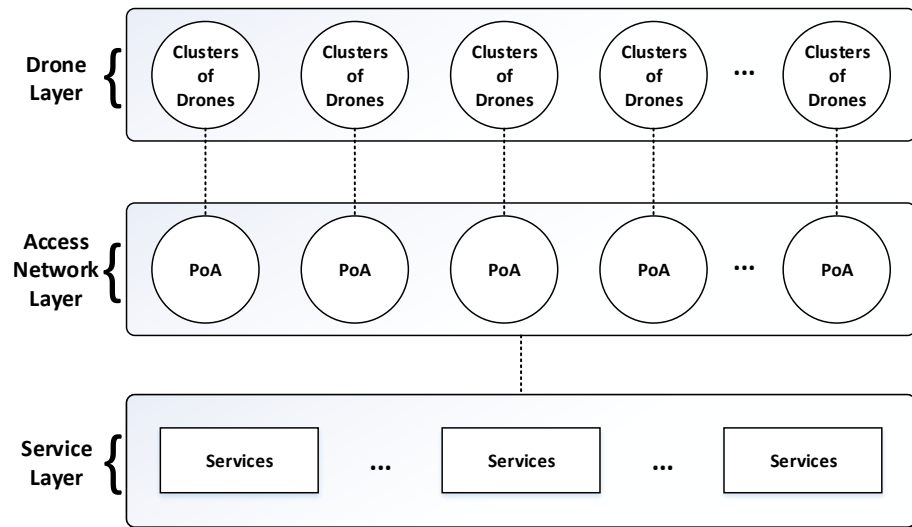


Figure 1. The design of the proposed GHO scheme.

To create clusters of drones, each PoA applies Formula (1) and calculates the number of segments A to which the underlying geographical area should be divided. In this formula, the parameter $Cluster_{RP}$ represents the target percentage of drones that should participate in each cluster.

$$A = 1/Cluster_{RP} \quad (1)$$

It is noted that the flying position of each drone affects the creation of the cluster of drones in each segment. In addition, a unique identifier (ID) is generated for each cluster. The aforementioned procedure is executed three times, since three different altitude ranges are considered for the drones' flights: low, medium, and high altitude (Algorithm 1).

Algorithm 1 Creation of the clusters of drones.

```

Define three distinct level of altitudes: Low, Medium and High
for each level of altitude do
  Define the target  $Cluster_{RP}$ 
  Calculate the number of segments ( $A$ ) using (1)
  for each  $A_i$  segment do
    Create a cluster containing the drones that are flying inside to its territory
  end for
end for

```

3.3. Cluster Head Election

The election of a CH is one of the most important functions of the proposed algorithm. Initially, for each cluster A_i the corresponding PoA calculates the center ($centre_{point}$). Thereafter, for the current time t , each drone calculates a score as follows:

$$CH_{score}[t] = \alpha \cdot Distance_{norm}[t] + \beta \cdot RSS_{norm}[t] + \gamma \cdot Direction[t] + \delta \cdot ETC \quad (2)$$

where the $Distance_{norm}[t]$ parameter indicates the normalized value of the distance of the drone from the $centre_{point}$, the $RSS_{norm}[t]$ is the normalized value of the signal strength that the drone receives from its current PoA, the $Direction[t]$ indicates the movement direction of the drone with respect to the $centre_{point}$, and the ETC represents the expected transmission count [31] or, in other words, the quality of bidirectional links that affect the lifetime of the cluster.

Regarding the estimation of the aforementioned parameters, it is noted that the $Distance_{norm}[t]$ parameter is calculated using (3), where the $Distance[t]$ parameter represents the exact distance of the drone from the $centre_{point}$, and the $Distance_{max}$ represents

the maximum distance that the drone can be from the $centre_{point}$, namely the radius of the corresponding cluster. Correspondingly, the $Distance[t]$ parameter is estimated using (4), where the $x_i[t]$, $y_i[t]$, and $z_i[t]$ parameters indicate the current geographic latitude, the current geographic longitude, and the current altitude of the drone. Similarly, in this formula, the x_j , y_j , and z_j parameters indicate the corresponding coordinates of the $centre_{point}$. Additionally, the $RSS_{norm}[t]$ parameter is calculated using (5), where the $RSS[t]$ represents the current strength of the signal that the drone receives from its PoA, and the RSS_{max} is the higher value of the signal strength that has been observed for the entire access network environment until the current time t . In addition, the $Direction$ parameter is calculated using (6) and obtains: (a) a positive value as long as the drone approaches the $centre_{point}$, (b) a negative value as long as the drone moves from the $centre_{point}$, and (c) a zero value as long as the drone remains stationary. Additionally, the ETC parameter is estimated using (7), where d_f and d_r represent the percentage of successful transmission and reception messages, respectively. Thus, the optimal value of the ETC could be equal to 0.5 for $d_f = 1$ and $d_r = 1$. Overall, the drone that obtains the higher score is elected as the CH of its cluster (Algorithm 2).

$$Distance_{norm}[t] = \frac{Distance[t]}{Distance_{max}} \quad (3)$$

$$Distance[t] = \sqrt{(x_i[t] - x_j)^2 + (y_i[t] - y_j)^2 + (z_i[t] - z_j)^2} \quad (4)$$

$$RSS_{norm}[t] = \frac{RSS[t]}{RSS_{max}} \quad (5)$$

$$Direction[t] = Distance_{norm}[t - 1] - Distance_{norm}[t] \quad (6)$$

$$ETC = \frac{1}{d_f + d_r} \quad (7)$$

Additionally, the parameters α , β , γ , and δ are weighting factors and thus $0 \leq \alpha \leq 1$, $0 \leq \beta \leq 1$, $0 \leq \gamma \leq 1$, $0 \leq \delta \leq 1$, and $\alpha + \beta + \gamma + \delta = 1$. The Analytic Network Process (ANP) [32] method is used for their calculation. The ANP analyzes the problem as a network of nodes, where each node represents a parameter, and the arcs between the nodes denote interactions between them. In addition, the ANP organized the parameters-nodes into clusters according to their type, while arcs within clusters are called inner dependencies, and arcs between clusters are called outer dependencies. Indicatively, in our case, we consider two clusters of parameters. The first cluster includes technical characteristics, namely the RSS and the ETC parameters. Accordingly, the second cluster includes movement characteristics, namely the $Distance$ and the $Direction$ parameters.

To perform its task, the ANP initially creates a pairwise comparison matrix A for each cluster of parameters using the nine-point importance scale presented in Table 1 [33]. The form of the A matrix is expressed as follows:

$$A = \begin{bmatrix} 1 & \dots & a_{1j} & \dots & a_{1p} \\ \vdots & & \vdots & & \vdots \\ 1/a_{1i} & \dots & 1 & \dots & a_{ip} \\ \vdots & & \vdots & & \vdots \\ 1/a_{1np} & \dots & 1/a_{jp} & \dots & 1 \end{bmatrix} \quad (8)$$

while p denotes the number of the parameters of the cluster. It is noted that in our case, during the instantiation of the system, the considered parameters are supposed to obtain equal importance with each other.

Subsequently, the geometric mean r_{A_i} of each row i in A is calculated using (9)

$$r_{A_i} = (a_{i1} \cdot a_{i2} \cdot \dots \cdot a_{ip})^{\frac{1}{p}}. \quad (9)$$

Then, the priority vector Ω_i of each cluster parameter is created as follows:

$$\Omega_i = [\omega_1 \quad \omega_2 \quad \dots \quad \omega_p] \tag{10}$$

where each ω_i is estimated using (11)

$$\omega_i = r_{A_i} / (r_{A_1} + r_{A_2} + \dots + r_{A_i} + \dots + r_{A_p}). \tag{11}$$

Table 1. The nine-point importance scale used for the construction of the pairwise matrix.

Relative Importance Value	Definition
1	Equal Importance
3	Moderate Importance
5	Strong Importance
7	Very Strong Importance
9	Extreme Importance
2, 4, 6, 8	Intermediate Values of Relative Importance

Algorithm 2 Election of the CH for each cluster.

```

for each cluster do
    Estimate  $centre_{point}$  of the cluster
    for each drone of the cluster do
        Obtain the coordinates  $x_i, y_i$  and  $z_i$  of its position
        Estimate its normalized distance from the  $centre_{point}$  using (3)
        Estimate the normalized RSS that it perceives from its current PoA using (5)
        Obtain its movement direction with respect to the  $centre_{point}$  using (6)
        Estimate the Expected Transmission Count (ETC) factor using (7)
        Calculate the score of the drone using (2)
    end for
    Elect the drone with the higher score as CH
end for
    
```

Next, the ANP creates a supermatrix W representing the inner and outer dependencies of the ANP network. This is a partitioned matrix, with each matrix segment representing the relationship between two clusters of parameters. To construct the supermatrix, the local priority vectors Ω are grouped and placed in the appropriate positions in the supermatrix based on the flow of influence from one cluster to another. Indicatively, if we assume a network of q clusters where each cluster $C_k, k = [1, 2, \dots, q]$ contains p_k parameters, denoted as $e_{k1}, e_{k2}, \dots, e_{kp_k}$, then the supermatrix is expressed as:

$$\tilde{W} = \begin{matrix} & & C_1 & \dots & C_k & \dots & C_q \\ & & e_{11} \dots e_{1p_1} & \dots & e_{k1} \dots e_{kp_k} & \dots & e_{q1} \dots e_{qp_q} \\ C_1 & \begin{bmatrix} \vdots \\ e_{1p_1} \\ \vdots \\ e_{k1} \\ \vdots \\ e_{kp_k} \\ \vdots \\ e_{q1} \\ \vdots \\ e_{qp_q} \end{bmatrix} & \begin{bmatrix} W_{11} & \dots & W_{1j} & \dots & W_{1q} \\ \vdots & \vdots & \vdots & \vdots & \vdots \\ W_{k1} & \dots & W_{kj} & \dots & W_{kq} \\ \vdots & \vdots & \vdots & \vdots & \vdots \\ W_{q1} & \dots & W_{qj} & \dots & W_{qq} \end{bmatrix} & & & \end{matrix} \tag{12}$$

Then, the supermatrix is transformed to a stochastic one, namely the Weighted Supermatrix W' , using (13).

$$W'_{k,j} = W_{k,j}/q \quad (13)$$

Finally, the Weighted Supermatrix is raised to limiting powers, namely it is multiplied by itself, until all the entries converge and all the columns of the produced Limited Supermatrix become same, and their values show the weight of each parameter.

3.4. Mobility Management

The proposed mobility management methodology presented in Figure 2 is based on the Fast Proxy Mobile IPv6 (FPMIPv6) and Media Independent Handover (MIH) protocols. More specifically, FPMIPv6 offers solutions in heterogeneous terminal mobility environments by supporting a variety of different technologies. It also provides a common communication channel to quickly relay the appropriate signaling messages. Nevertheless, by only leveraging FPMIPv6, a satisfactory environment for initializing the transmission and selecting the next network cannot be provided. FPMIPv6 is actually characterized by a lack of relay initiation events, as well as a lack of procedures for searching and selecting candidate networks for relaying. Finally, control HO steps to the candidate network and link-level processes are not guaranteed. Consequently, the use of FPMIPv6 together with the MIH protocol is suggested to satisfactorily handle the aforementioned issues. Indeed, their combination consistently appears in the literature to permanently solve mobility issues, such as relay mis-initialization, failed HO to the new network, or the ping-pong effect.

3.4.1. HO Initiation

During this phase, the data rate $C_{j,i}$ of the j th Cluster Head (CH) from the current PoA is continuously monitored, as proposed in [34]. More specifically, $C_{j,i}$ depends on the bandwidth $B_{j,i}$ and on the Signal to Interference plus Noise Ratio $SINR_{j,i}$, and according to Shannon's theorem, $C_{j,i}$ is calculated as follows:

$$C_{j,i} = \sum_{s=1}^S (B_{s,j,i} \cdot \log_2(1 + SINR_{j,i}) \cdot W_s) \quad (14)$$

where the parameter W_s indicates the relative importance of each service s . As long as the CH of cluster A_i with ID_i perceives that the received data rate $C_{j,i}$ is below a certain threshold, it sends a `1.MIH_Data_Rate_Going_Down` message to the current Mobile Access Gateway (MAG) to initiate an HO for its cluster. In this message, the required data rate that the next network is requested to provide, as well as the identifiers of each Cluster Member (CM), are passed as parameters. Then, the current MAG starts buffering the received packets from the Local Mobility Anchor/Authentication, Authorization, and Accounting (LMA/AAA) entity.

3.4.2. Network Selection

During the network selection, the current MAG sends a `2.MIH_GET_Information` request message containing information about the minimum acceptable data rate for the collection of information about the candidate networks at the given time instance to the Media Independent Handover Information Services (MIIS) entity of the Software Defined Networking (SDN) controller. Subsequently, the SDN controller retrieves information about the candidate networks satisfying the required data rate and applies the Simple Additive Weighting (SAW) [35] method to rank these networks. In particular, the SDN controller uses (15) in order to estimate a score for each available PoA. It is noted that the $C_{i,s}$, the $P_{i,s}$, the $L_{i,s}$, and the $J_{i,s}$ parameters indicate the normalized values about the data rate, the packet loss, the latency, and the jitter that the i th PoA offers for the s th service, respectively, while the $W_{C,s}$, the $W_{P,s}$, the $W_{L,s}$, and the $W_{J,s}$ represent the corresponding relative importance of the aforementioned parameters for each service, calculated using the ANP method. Then, a sorted candidate networks list is created and transmitted to the current

MAG using a 3.*MIH_GET_Information_response* message. The current MAG checks the resources of each candidate MAG by exchanging 4.*MIH_N2N_HO_Resource_request* and 5.*MIH_N2N_HO_Resource_response* messages. Note that the above process is repeated until a MAG with the required resources is found.

$$SAW_i = \sum_{s=1}^S (C_{i,s} \cdot W_{C,s} + P_{i,s} \cdot W_{P,s} + L_{i,s} \cdot W_{L,s} + J_{i,s} \cdot W_{J,s}) \quad (15)$$

3.4.3. HO Execution

During the HO execution, the current MAG first commits the resources to the new MAG for the upcoming HO by exchanging the 6.*MIH_N2N_HO_Commit_request* and 7.*MIH_N2N_HO_Commit_response* messages. Then, for the commitment of the resources of the new MAG, the CH of the cluster sends the 8.*MIH_Net_HO_Commit_request* message. Thereafter, the CH receives the message 9.*MIH_Net_HO_Commit_response* which confirms that the required resources are committed to the new MAG. Then, the current MAG informs the new MAG with relevant information for both the CH and the CMs of the cluster with the respective drone ID, drone-ID Logical Link Identifier, and the LMA/AAA from which data traffic is forwarded to the drones with the message 10.*Handover_Initiate*. When the message is successfully received, the new MAG responds with 11.*Handover_Acknowledgment* to the CH, while the CH forwards this message to the CMs of his cluster. At the same time, a bidirectional tunnel is established between the MAGs to send a copy of the packets that were buffered during the initiation of the HO. These data will be sent later, as long as the CH and the CMs are connected to the new MAG. As a result, the new MAG sends a Proxy Binding Update (PBU) message, namely the 12.*PBU*, to the LMA/AAA to create a transient entry in the Binding Cache Entry (BCE) by entering information about the MAGs affiliated with the drones, the home network prefix, as well as the active flags, namely the Buffering (B), the Transient (T), the Proxy (P) and the Forward (F) flags. When the LMA/AAA successfully receives the PBU, it starts buffering the packets from the network.

Now that the transient registration is registered in the BCE, a Proxy Binding Acknowledgment (PBA) message, namely the 13.*PBA*, is sent to the new MAG to establish the bidirectional tunnel between these two entities. Subsequently, the downlink packets are destined by the LMA/AAA for the new MAG where they are buffered until the CH and CMs are connected to the new MAG. Specifically, the bidirectional tunnel between the LMA/AAA and the new MAG remains active until the transient registration is changed to permanent. Therefore, transient registration allows for a smoother transition from the current MAG to the new MAG by avoiding packet loss phenomena and HO failures. Both the CH and the CM send 14.*MIH_Link_up* messages via the locally installed Media Independent Handover Function (MIHF) entity to inform the new PoA that they can receive packets through the communication channel. Additionally, the CMs send the 15.*UNA* message to the new MAG to inform the new PoA that the link and the Internet Protocol (IP) layers are established. The new MAG re-exchanges the 16.*PBU* and 17.*PBA* messages for each cluster entity, such that the entries from transients are permanent. Moreover, the resources of the current MAG are released by exchanging the 18.*MIH_N2N_Complete_request* and 19.*MIH_N2N_Complete_response* messages. Finally, the two-way tunnel, which ensures smoother transition to the new MAG is abandoned and packets reach their destination from the new MAG.

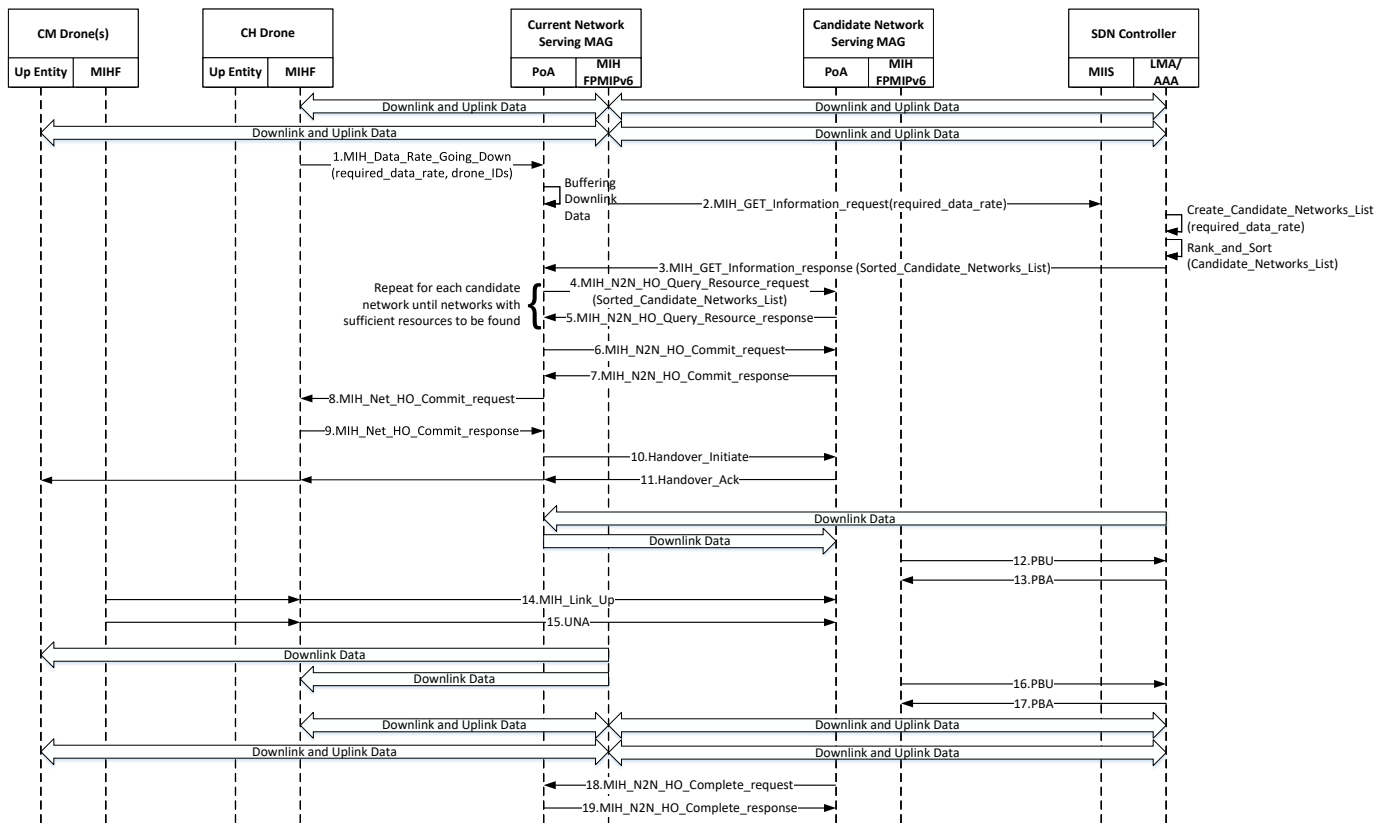


Figure 2. The signaling performed by the proposed GHO scheme.

4. Simulation Setup and Results

In order to carry out the simulation procedure, a Fog infrastructure consisting of a set of PoAs is initially created. Specifically, the Fog includes two LTE-A Pro with Full Dimensional Multiple Input Multiple Output (FD-MIMO) macrocells, four WAVE RSUs, two LTE-A femtocells, and two WiMAX femtocells. The coverage radius of the macrocells is equal to 1000 m, the radius of the WAVE RSUs is equal to 200 m, and the radius of the LTE-A or WiMAX femtocells is equal to 100 m. Each LTE-A Pro FD-MIMO Macrocell offers $B_i = 100$ MHz bandwidth, each WAVE RSU offers $B_i = 10$ MHz, and each LTE-A or WiMAX Femtocell offers $B_i = 20$ MHz. Additionally, a set of 300 drones is moving inside the coverage area of the network access environment. Initially, each LTE-A Pro FD-MIMO macrocell serves 100 of the aforementioned drones, each WAVE RSU serves 15 drones, and each LTE-A or WiMAX femtocell serves 10 drones. Additionally, three flying altitudes are considered for the drones, namely low, medium, and high altitude, while the simulated drones are equally distributed to these altitudes. Indicatively, for the cases of each LTE-A Pro FD-MIMO macrocell, 34 drones fly at low altitude, 33 drones fly at medium altitude, and 33 drones fly at high altitude. In addition, the Cloud infrastructure includes a set of Virtual Machines (VMs) providing video streaming and IoT services. The entire simulation blueis created using the Network Simulator 3 (NS3) [36], while the total simulation duration is equal to 200 s. Figure 3 depicts the simulated topology.

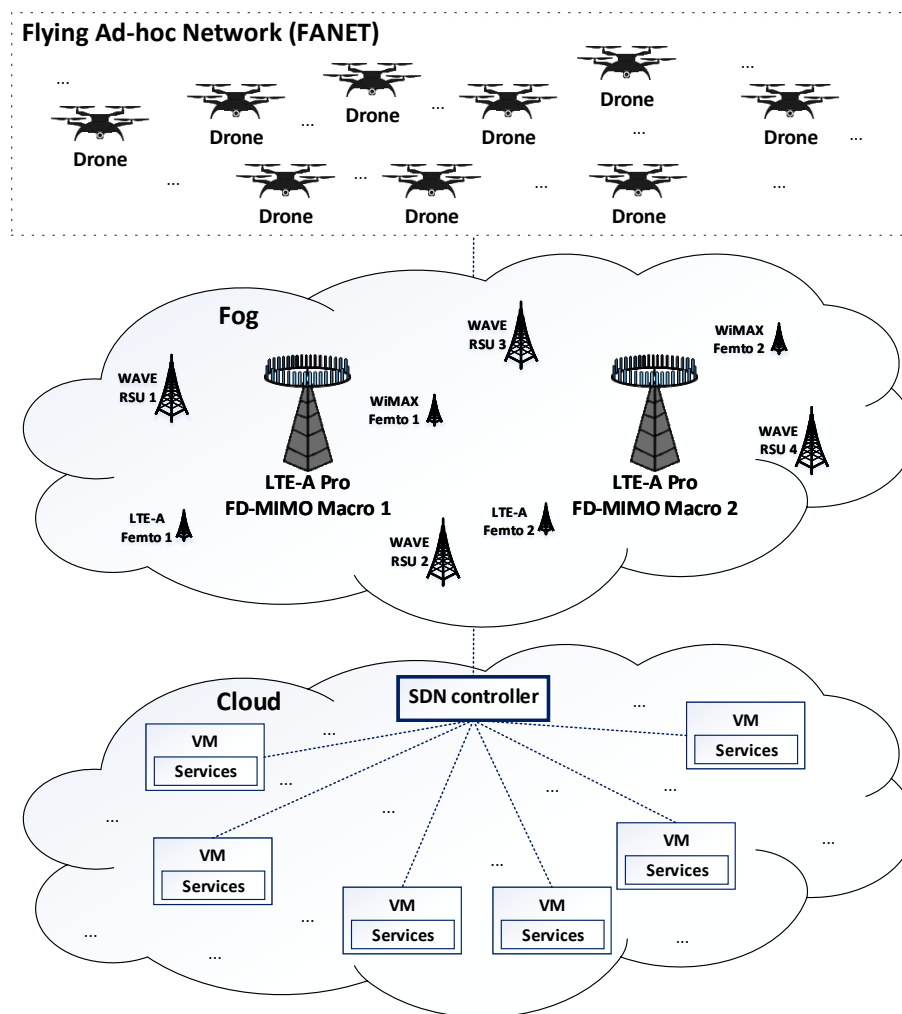


Figure 3. The simulated topology used for the evaluation of the proposed GHO scheme.

Initially, for each flying altitude, each PoA estimates the number of drones ($D_{Density}$) flying inside its coverage area, while at the same time the target percentage of drones to each cluster ($Cluster_{RP}$) is supposed to be equal to 0.11. Then, each PoA calculates the number of segments (A) that should be created to each flying altitude using (1). Subsequently, a cluster of drones is created in each segment containing the drones flying inside the segment. After the formation of clusters of drones, a CH is elected for each cluster using the algorithm described in Section 3.1, by assuming that the *Distance*, *RSS*, *Direction*, and *ETC* parameters obtain equal importance with each other, namely $\alpha = \beta = \gamma = \delta = 0.25$. Indicatively, Figure 4 illustrates the clusters created from the LTE-A Pro FD-MIMO 1 macrocell when the simulation time becomes equal to 100 s. In this figure, the blue points represent the center of each cluster, while each green drone corresponds to the elected CH of each cluster. One observes that there exist nine created clusters in each flying altitude, while a cluster id is assigned to each cluster.

Table 2 shows the results for the cluster with id equal to $m.5$ which is centered at the coordinates (500.0, 500.0, 500.0).

Table 2. The results for the cluster with id equal to $m.5$.

Drone ID	Drone Coordinates (x,y,z)	Distance [t]	RSS [t]	Direction [t]	ETC	Cluster Head (CH)
d49	(416,487,485)	86.313 m	−71 dB	0.1	0.5	No
d50	(503,585,581)	117.452 m	−70 dB	0	0.5	No
d51	(509,483,482)	26.343 m	−68 dB	0.2	0.5	Yes

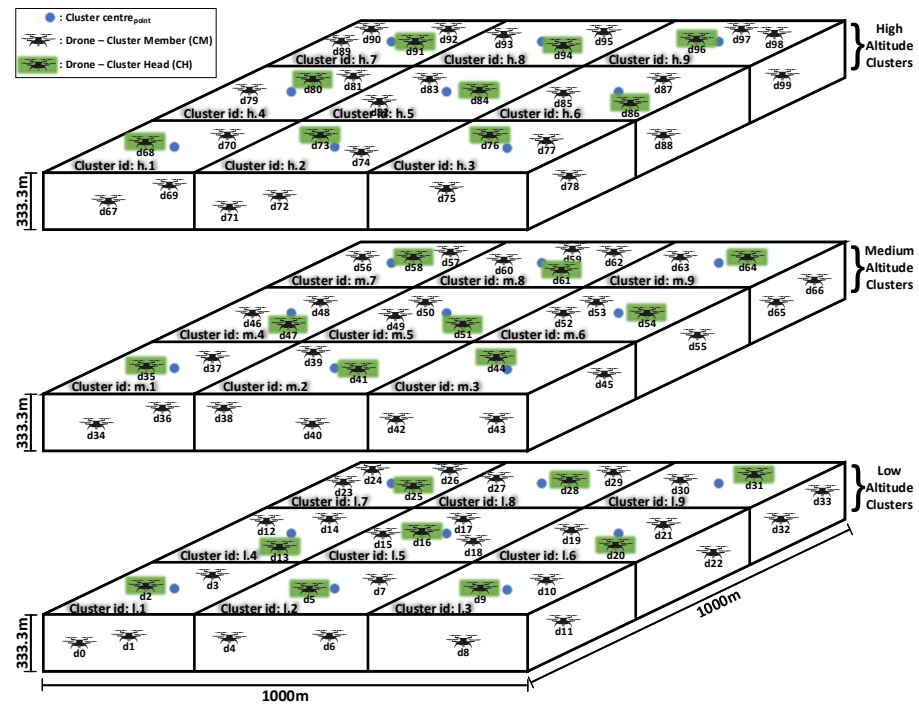


Figure 4. The clusters created from the LTE-A Pro FD-MIMO 1 macrocell.

Table 3 presents the simulation parameters, and Table 4 demonstrates the cost of each signaling message that can be exchanged between the network components during the mobility management.

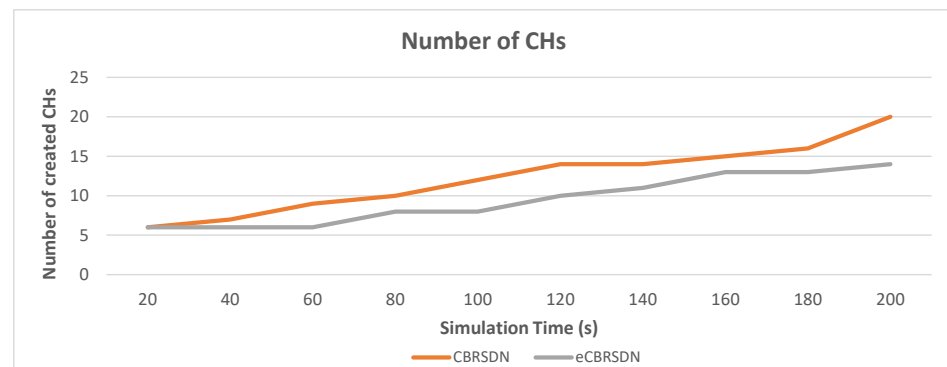
Table 3. Simulation parameters.

Abbreviation	Value	Description
Simulation time	200 s	The duration of the simulation
$Cluster_{RP}$	0.11	Target percentage of drones to each cluster
h_{macro}	1000 m	Height of macrocell coverage area
w_{macro}	1000 m	Radius of macrocell coverage area
h_{rsu}	200 m	Height of RSU coverage area
w_{rsu}	200 m	Radius of RSU coverage area
h_{femto}	100 m	Height of femtocell coverage area
w_{femto}	100 m	Radius of femtocell coverage area
u	10–40 m/s	Velocity of drones
D_{total}	300	Total number of drones
$D_{total,macro}$	100	Initial number of drones per macrocell
$D_{total,rsu}$	15	Initial number of drones per RSU
$D_{total,femto}$	10	Initial number of drones per femtocell
P_f	0.5 [37]	Frame Error Rate
H_{MN_MAG}	1 hop	Distance between drone (either CH or CM) and MAG
H_{MAG_LMA}	1 hop	Distance between MAG and LMA/AAA
H_{MAG_MIIS}	1 hop	Distance between MAG and MIIS
H_{MAG_MAG}	1 hop	Distance between MAG and MAG

Table 4. Signaling costs.

Message	Cost	Abbreviation
<i>MIH_Link_Going_down</i>	78	M1
<i>MIH_Link_up</i>	95	M2
<i>MIH_Get_Information_request</i>	1500	M3
<i>MIH_Get_Information_response</i>	1500	M4
<i>MIH_Net_HO_Candidate_Query_request</i>	$63 + 118n + 8 \cdot m \cdot n$	M5
<i>MIH_Net_HO_Candidate_Query_response</i>	$77 + 101 \cdot m$	M6
<i>MIH_N2N_HO_QueryResource_request</i>	$150 + 11 \cdot m$	M7
<i>MIH_N2N_HO_QueryResource_response</i>	165	M8
<i>MIH_N2N_HO_Commit_request</i>	213	M9
<i>MIH_N2N_HO_Commit_request(Extended)</i>	264	M9e
<i>MIH_N2N_HO_Commit_response</i>	92	M10
<i>MIH_N2N_HO_Commit_response(Extended)</i>	92	M10e
<i>MIH_Net_HO_Commit_request</i>	122	M11
<i>MIH_Net_HO_Commit_response</i>	103	M12
<i>MIH_N2N_HO_Complete_request</i>	109	M13
<i>MIH_N2N_HO_Complete_response</i>	112	M14
<i>MIH_MN_HO_Commit_request</i>	75	M15
<i>MIH_MN_HO_Commit_response</i>	78	M16
AAA Query	32	M17
AAA Reply	60	M18
<i>Handover_Initiate</i> (HI)	72	M_{HI}
<i>Handover_Ack</i> (Hack)	32	M_{Hack}
PBU	76	M_{PBU}
PBA	52	M_{PBA}
RS	16	M_{RS}
RA	64	M_{RA}
UNA	52	M_{UNA}

The proposed eCBRSN scheme is compared with the original CBRSN [24] algorithm in terms of the average number of the CHs elected per PoA during the simulation, as well as in terms of the lifetime of the elected CHs. In particular, the original algorithm tends to elect drones as CHs without taking into consideration factors such as the movement direction or the quality of the communication link. Thus, in cases where the candidate drones move away the *centrepoint* of their cluster, or in cases where the quality of the communication link is poor, the proposed scheme performs better than the CBRSN algorithm. More specifically, during the 200 s of the simulation, the CBRSN algorithm elected 20 different CHs on average per PoA, while the proposed one elects 14 on average per PoA (Figure 5), indicating less CH election overhead to the entire system. It is noted that the number of clusters within the entire simulation remained constant for both algorithms.

**Figure 5.** The number of created CHs for each algorithm.

Additionally, the results reveal how the lifetime of the elected CHs is affected from the average speed of the drones. In particular, the proposed eCBRSDN algorithm increases the lifetime of the elected CHs, enhancing the stability of the clusters by changing their CH fewer times. This situation occurs since the proposed algorithm takes into consideration the movement direction of each candidate CH during the selection of the CH for each cluster. Specifically, as illustrated in Figure 6, the average CH lifetime decreases for both algorithms as the movement speed of the drones increases from 10 m/s and up to 40 m/s. However, the proposed eCBRSDN algorithm achieves higher CH lifetimes in all cases, with the difference of the average CH lifetime becoming up to 6 s where the average speed of the drones becomes 40 m/s.

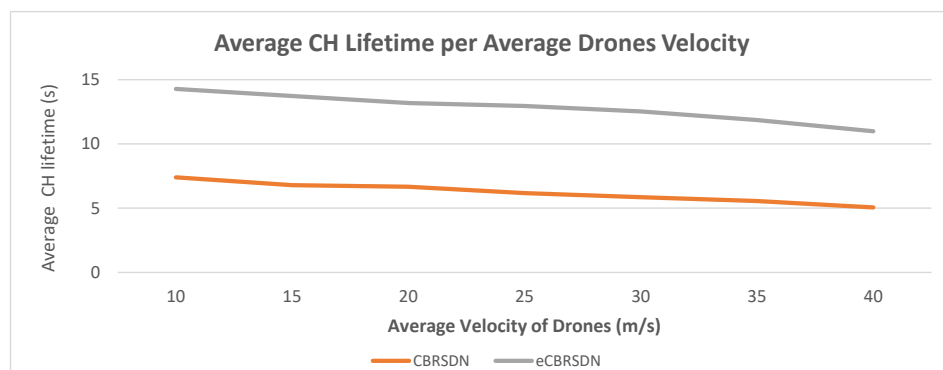


Figure 6. The average lifetime of CHs regarding the average velocity of drones.

Furthermore, the efficiency of the HO initiation and the network selection, as well as the HO signaling cost [38] of the proposed scheme is compared with the ones achieved by the Mobile IP (MIP) [39], the Fast HO [40], the Fast Proxy Mobile IPv6 (FPMIPv6) [41], and the Enhanced Fast Proxy Mobile IPv6 (eFPMIPv6) [42,43] schemes.

For the calculation of the $C_{j,Video,i}$ and $C_{j,IoT,i}$ values during the HO initiation process, the relative importance W_s of each service is estimated using the respective service priority constraints defined in the LTE QoS class specifications [44,45]. Thus, we obtain $W_{Video} = 0.43$ and $W_{IoT} = 0.57$. Accordingly, the threshold values are calculated by considering $SINR = 14$ db as proposed in [46]. Thus, we obtain $C_{Threshold,Video} = 0.812845$ and $C_{Threshold,IoT} = 1.077493$, whereas the overall HO initiation threshold is $C_{Threshold} = C_{Threshold,Video} + C_{Threshold,IoT} = 1.890338$. When the observed $C_{j,s,i}$ of a CH drops below the specified threshold, the drones of the corresponding cluster should perform an HO. Indicatively, Table 5 presents the HO initiation parameters of each CH of the low altitude clusters of the LTE-A Pro FD-MIMO 1 macrocell for a simulation time of 100 s.

Table 5. The HO initiation parameters of each CH of the low altitude clusters of the LTE-A Pro FD-MIMO 1 macrocell at a simulation time of 100 s.

Cluster ID	1.1	1.2	1.3	1.4	1.5	1.6	1.7	1.8	1.9
CH	d2	d5	d9	d13	d16	d20	d25	d28	d31
SINR _{j,i} (dB)	5.3488	9.3478	10.952	13.529	19.166	15.333	14.375	12.777	6.9696
C _{Video,j,i}	0.3192	5.3100	0.6503	7.9691	2.1816	1.795	1.6885	0.7617	0.4167
C _{IoT,j,i}	0.4231	7.0389	0.862	10.563	2.8919	2.3794	2.2383	1.0097	0.5524
C _{sum,j,i}	0.7423	12.349	1.5123	18.532	5.0735	4.1745	3.9268	1.7715	0.9692
HO required	yes	no	yes	no	no	no	no	yes	yes

It is noted that the MIP, Fast HO, FPMIPv6, and eFPMIPv6 schemes implement RSS-based HO initiation and network selection [47]. Figure 7 presents the average data rate indicator value (C) observed for each HO scheme and obtained via the HO initiation and network selection processes, namely the proposed one and the RSS-based one implemented

by the aforementioned existing schemes. Clearly, the proposed GHO scheme achieves higher average data rate values in all cases.

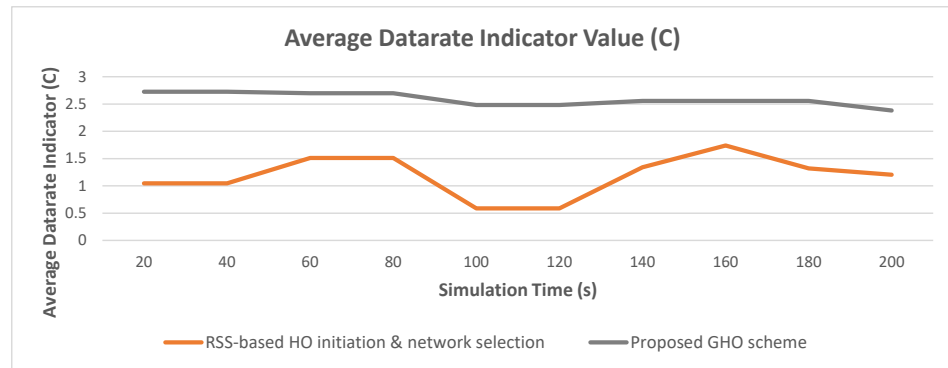


Figure 7. The average data rate indicator value (C) observed for each HO scheme.

The signaling cost for the proposed GHO scheme for each cluster of drones is estimated as follows:

$$S_{proposed} = \frac{P_f}{1 - P_f} \cdot H_{MN_MAG} \cdot (M_1 + M_{11} + M_{12} + M_{HACK} + cms \cdot (M_2 + M_{UNA})) + H_{MAG_MAG} \cdot (m \cdot (M_7 + M_8) + M_9 + M_{10} + M_{HI} + M_{HACK} + M_{13} + M_{14}) + H_{MAG_MIIS} \cdot (M_3 + M_4) + 2 \cdot cms \cdot H_{MAG_LMA} \cdot (M_{PBU} + M_{PBA}) \quad (16)$$

where the P_f parameter represents the connection failure probability, which in our work is supposed to be equal to 0.5 [37]. In addition, the cms parameter indicates the number of the CMs, the H_{MN_MAG} is the number of hops between a drone (either a CH or a CM) and its current MAG, H_{MAG_MAG} is the number of hops between two MAGs of the simulated topology, H_{MAG_MIIS} is the number of hops between a MAG and the MIIS, and H_{MAG_LMA} is the corresponding number of hops between a MAG and the LMA/AAA. Furthermore, it is considered that $H_{MN_MAG} = 1$, $H_{MAG_MAG} = 1$, $H_{MAG_MIIS} = 1$, and $H_{MAG_LMA} = 1$, while the m parameter represents the number of the candidate MAGs. In addition, the signaling cost of the MIP scheme is calculated for each individual drone (this scheme does not perform clustering of drones) as follows:

$$S_{MIP} = \frac{P_f}{1 - P_f} \cdot H_{MN_MAG} \cdot (M_3 + M_4 + M_5 + M_6 + M_{15} + M_{16} + M_{RS} + M_{RA}) + H_{MAG_MAG} \cdot (m \cdot (M_7 + M_8) + M_9 + M_{10} + M_{13} + M_{14}) + H_{MAG_MIIS} \cdot (M_3 + M_4) + H_{MAG_LMA} \cdot (3 \cdot (M_{PBU} + M_{PBA}) + M_{17} + M_{18}) \quad (17)$$

Similarly, the signaling cost per drone of the Fast HO scheme is estimated as:

$$S_{FastHO} = \frac{P_f}{1 - P_f} \cdot H_{MN_MAG} \cdot (M_1 + M_2 + M_{11} + M_{12} + M_{UNA}) + H_{MAG_MAG} \cdot (m \cdot (M_7 + M_8) + M_9 + M_{10} + M_{HI} + M_{HACK} + M_{13} + M_{14}) + H_{MAG_MIIS} \cdot (M_3 + M_4) + 2 \cdot H_{MAG_LMA} \cdot (M_{PBU} + M_{PBA}) \quad (18)$$

while the corresponding signaling cost of the FPMIPv6 scheme is estimated as:

$$S_{FPMIPv6} = \frac{P_f}{1 - P_f} \cdot H_{MN_MAG} \cdot (M_1 + M_5 + M_6 + M_{11} + M_{12} + M_{RS} + M_{RA}) + H_{MAG_MAG} \cdot (m \cdot (M_7 + M_8 + M_9 + M_{10} + M_{13} + M_{14} + M_{HI} + M_{Hack})) + H_{MAG_MIIS} \cdot (M_3 + M_4) + 3 \cdot H_{MAG_LMA} \cdot (M_{PBU} + M_{PBA}) \quad (19)$$

In addition, the signaling cost per drone of the eFPMIPv6 scheme is estimated as follows:

$$S_{eFPMIPv6} = \frac{P_f}{1 - P_f} \cdot H_{MN_MAG} \cdot (M_1 + M_2 + M_5 + M_6 + M_{11} + M_{12} + M_{UNA}) + \\ H_{MAG_MAG} \cdot (m \cdot (M_7 + M_8) + M_{9e} + M_{10e} + M_{13} + M_{14}) + \\ H_{MAG_MIIS} \cdot (M_3 + M_4) + 2 \cdot H_{MAG_LMA} \cdot (M_{PBU} + M_{PBA}) \quad (20)$$

In general, the aforementioned schemes can achieve satisfactory signaling cost when they are applied for the manipulation of the increased mobility of individual drones in cases where the number of drones is low. However, as the number of drones increases, the proposed scheme achieves lower signaling cost since it exchanges fewer signaling messages than the other schemes. As the proposed scheme organizes the drones into clusters, the CH of each cluster exchanges some of the required signaling messages only one time on behalf of the entire drones of his cluster. More specifically, the first nine signaling messages of the proposed scheme, namely from the message 1. *MIH_Data_Rate_Going_Down* and up to the message 9. *MIH_Net_HO_Commit_responce*, are exchanged only one time, decreasing the overall signaling cost. On the other hand, the previously proposed schemes exchange similar signaling messages multiple times, namely one time for each individual drone, thus increasing the overall signaling cost.

As presented in Figure 8, the average signaling costs of the MIP, the Fast HO, the FPMIPv6, and the eFPMIPv6 schemes are equal to 357,680, 196,248, 265,478, and 261,188 Bytes, respectively. On the other hand, the proposed scheme achieves lower signaling cost which is equal to 18,700 Bytes, thus producing less signaling overhead during the mobility management process.

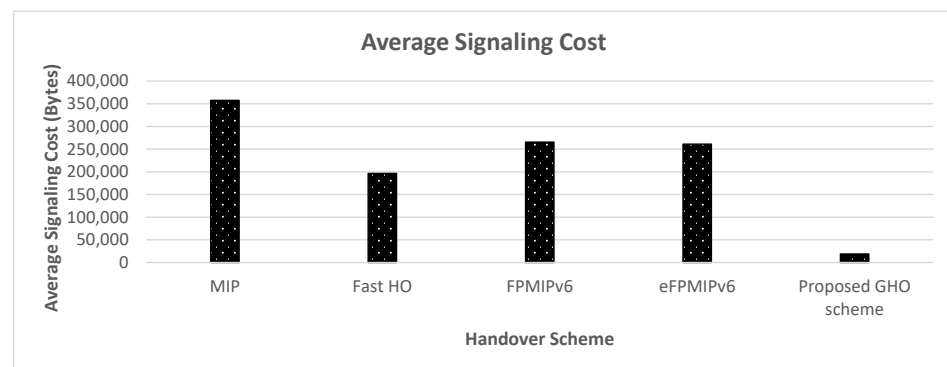


Figure 8. The average signaling cost observed for each HO scheme.

5. Testbed Deployment and Experimental Results

The proposed GHO scheme is also evaluated in real-world scenarios using a testbed that has been implemented in a controlled laboratory environment. Figure 9 presents the architecture of the implemented testbed which is based on the TP-Link Omada Cloud SDN platform [48]. Specifically, the network access environment consists of three TP-LINK EAP225 MU-MIMO outdoor PoAs [49]. In addition, a Huawei RH2288H V3 rack server [50] implements a Cloud infrastructure with a set of Virtual Machines (VMs) supporting video streaming services. In addition, in our testbed, the MAGs and the MIH FPMIPv6 entities of the PoAs, as well as the MIIS and the LMA/AAA entities of the SDN controller are also implemented as VMs on the aforementioned server. The PoAs and the VMs are connected to a TP-LINK T2600G-28TS Jetstream switch [51], while a TP-LINK OC200 cloud controller [52] along with the TP-Link Omada controller software [53] provide centralized control to the entire testbed architecture. Additionally, up to five Pixhawk Raspberry Pi drones [54] are initially connected to the LINK EAP225 MU-MIMO outdoor PoA 1, while each drone flies with constant velocity and streams live video to the corresponding VMs of the server. Table 6 presents the technical parameters of the implemented testbed.

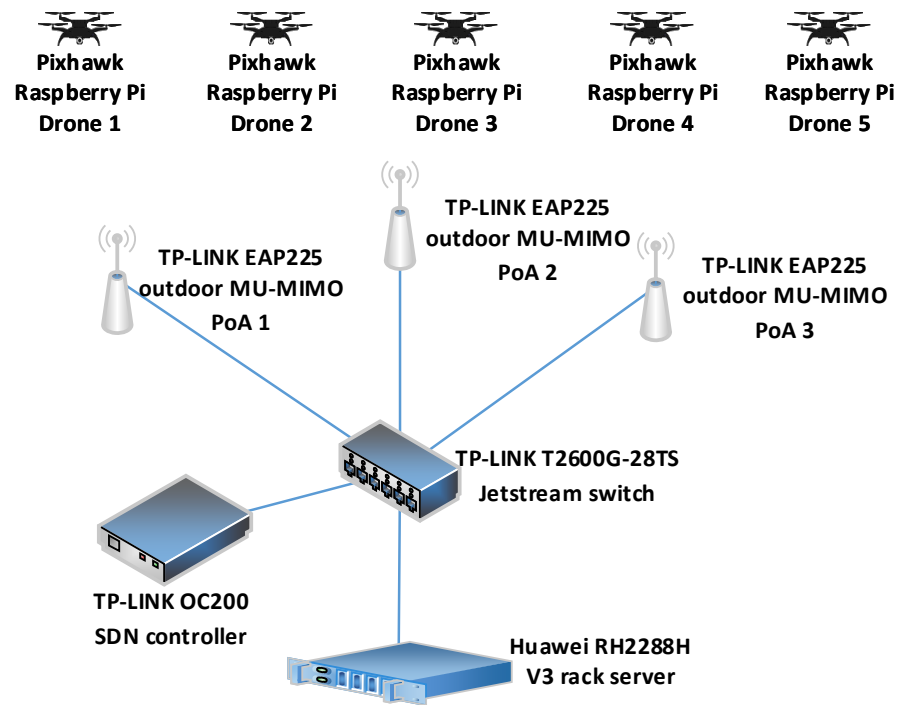


Figure 9. The architecture of the implemented testbed.

Table 6. The testbed parameters.

Model	Used Standard	Points of Access (PoAs)			Default Bandwidth	Max TX Rate *	TX Power
		Channel	Frequency				
TP-LINK EAP245 PoA 1	IEEE 802.11ac	52	5260 MHz		80 MHz	866.7 Mbps	25 dBm
TP-LINK EAP245 PoA 2	IEEE 802.11ac	64	5320 MHz		80 MHz	866.7 Mbps	25 dBm
TP-LINK EAP245 PoA 3	IEEE 802.11ac	100	5500 MHz		80 MHz	866.7 Mbps	25 dBm
* Regarding the Default Bandwidth							
Switch							
Model	Ports						
TP-LINK T2600G-28TS Jetstream	24 Gigabit Ethernet ports and 4 Small Form-factor Pluggable (SFP) 4 Gbps ports						
SDN Controller							
Model	Description						
TP-LINK OC200	Centralized Management of the Omada Cloud Platform, including the TP-LINK EAP PoAs						
Services							
Service	Specifications						
Realtime Video Streaming	4K video with 30 Frames per Second (FPS)						

To evaluate the proposed eCBRSN scheme using the testbed, an experimental scenario was performed for 120 s. In this experiment, the eCBRSN scheme is compared with the original CBRSN [24] scheme in terms of the average number of CHs elected. It is noted that, similar to the simulation setup described in the previous section, the eCBRSN scheme elects the CHs by assuming $\alpha = \beta = \gamma = \delta = 0.25$, namely the Distance, RSS, Direction, and ETC parameters obtain equal importance with each other. One observes

(in a similar basis to the simulation results presented in the previous section) that the CBRSDN algorithm tends to elect drones as CHs without considering factors such as the movement direction or the quality of the communication link. Thus, during the experiment, the CBRSDN algorithm elected eight different CHs on average per PoA while the proposed eCBRSN scheme elected three on average (Figure 10), indicating less CH election overhead to the entire system. It is noted that both algorithms were executed using exactly the same mobility pattern for the entire drones.

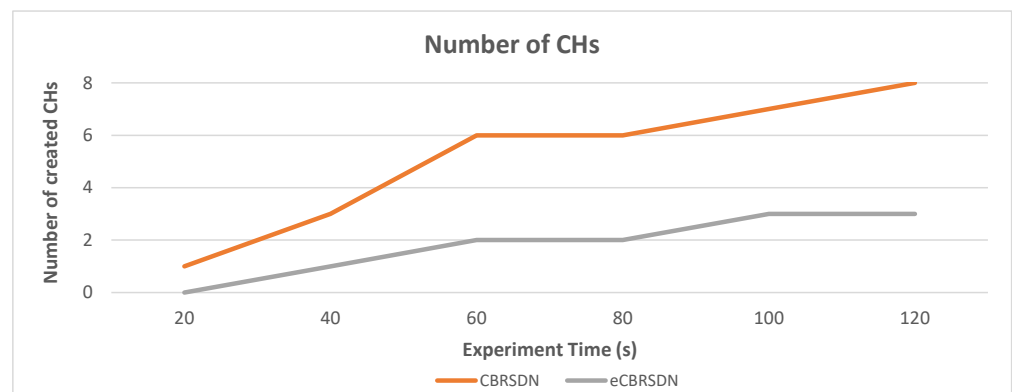


Figure 10. The number of created CHs for each algorithm during the experiment performed using the testbed.

Furthermore, similar to the previous section, the proposed scheme is evaluated and compared with the MIP, the Fast HO, the FPMIPv6, and the eFPMIPv6 schemes in terms of the average data rate indicator value (C) as well as in terms of the total signaling cost observed during the experiment performed using the testbed. According to Figure 11, the proposed scheme achieves higher values for the C indicator in all cases compared with the RSS-based methodology that is implemented by the aforementioned existing schemes.

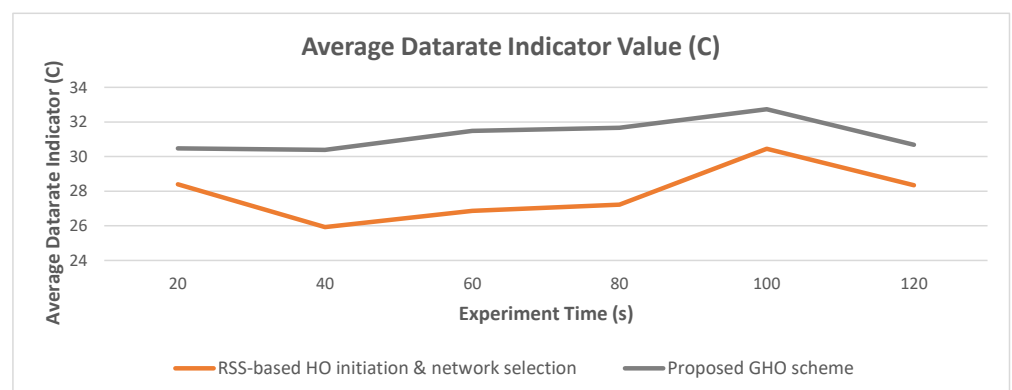


Figure 11. The average data rate indicator value (C) observed for each HO scheme during the experiment performed using the testbed.

Finally, Figure 12 indicates that the proposed scheme also outperforms the existing schemes in terms of the average cost of the signaling performed during our experiment. Specifically, the proposed scheme achieves lower signaling cost which is equal to 5445 Bytes, while at the same time the signaling costs of the MIP, the Fast HO, the FPMIPv6, and the eFPMIPv6 schemes are equal to 41,100, 25,050, 30,885, and 27,165 Bytes, respectively.

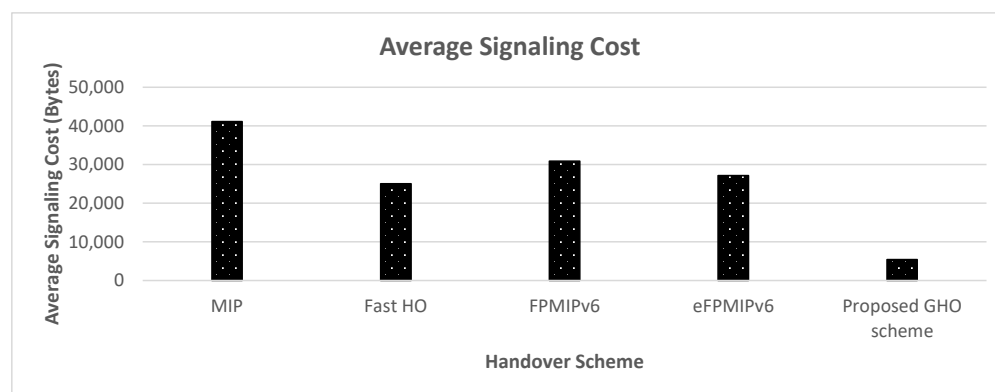


Figure 12. The average signaling cost observed for each HO scheme during the experiment performed using the testbed.

6. Conclusions

In this paper, a scheme for mitigating the connectivity issues in drone-aided networks has been presented. More specifically, an algorithm for efficiently creating clusters of drones has been proposed, along with a mechanism for electing a CH for each cluster. In addition, an algorithm for performing group HO has been described, including the HO initiation, the network selection, and the HO execution processes. The proposed scheme has been evaluated using simulations, where a next-generation drone-aided network architecture supporting IoT and multimedia services has been implemented. In addition, a testbed has been deployed in a controlled laboratory environment and provided results for a real-world experimental scenario. The access network environment of the simulated architecture consisted of IEEE 802.11p WAVE, LTE, and WiMAX PoAs. Both the simulation and experimental results showed that the proposed scheme outperforms existing methodologies in terms of the number of the required CHs, the average CH lifetime per drones' velocity, and the cost of the signaling performed during the mobility management.

Future work includes the further evaluation and optimization of the CH election procedure for specific cases of network topologies, where the considered parameters (namely the Distance, RSS, Direction, and ETC) should obtain different relative importance with each other. Indicatively, in network topologies where the drones remain stationary or move with very low velocities, the importance of the Direction is decreased. In addition, future work will include the enhancement of the proposed scheme using Machine Learning (ML) and Deep Learning (DL) techniques. In particular, DL can be used to add an artificially intelligent Mobility Management Entity (MME) to the network architecture. This MME could interact with the entire infrastructure by giving positive rewards to the corresponding network components (e.g., CHs, CMs, or PoAs), when the HOs are successful and negative rewards when HO failures occurred. Subsequently, the MME can adapt the overall HO policy based on the aforementioned interaction with the entire network architecture in order to optimize the HO procedure, increase the overall QoS, and also decrease the HO failures and ping-pong effect.

Author Contributions: conceptualization, E.S., I.K., E.T.M., A.M. and D.D.V.; investigation, E.S., I.K. and E.T.M.; supervision, A.M. and D.D.V.; visualization, E.S.; writing—original draft, E.S. and I.K.; writing—review and editing, E.S., I.K., E.T.M., A.M. and D.D.V. All authors have read and agreed to the published version of the manuscript.

Funding: This research was partially funded by the University of Piraeus Research Committee.

Data Availability Statement: Simulation data can be provided after contacting the corresponding author.

Acknowledgments: This work is partly supported by the University of Piraeus Research Committee.

Conflicts of Interest: The authors declare no conflict of interest.

References

1. Wheeb, A.H.; Nordin, R.; Samah, A.; Alsharif, M.H.; Khan, M.A. Topology-based routing protocols and mobility models for flying ad hoc networks: A contemporary review and future research directions. *Drones* **2021**, *6*, 9. [[CrossRef](#)]
2. Noor, F.; Khan, M.A.; Al-Zahrani, A.; Ullah, I.; Al-Dhlan, K.A. A review on communications perspective of flying ad-hoc networks: key enabling wireless technologies, applications, challenges and open research topics. *Drones* **2020**, *4*, 65. [[CrossRef](#)]
3. Ogbodo, E.U.; Abu-Mahfouz, A.M.; Kurien, A.M. A Survey on 5G and LPWAN-IoT for Improved Smart Cities and Remote Area Applications: From the Aspect of Architecture and Security. *Sensors* **2022**, *22*, 6313. [[CrossRef](#)]
4. Michailidis, E.T.; Vouyioukas, D. A Review on Software-Based and Hardware-Based Authentication Mechanisms for the Internet of Drones. *Drones* **2022**, *6*, 41. [[CrossRef](#)]
5. Colajanni, G.; Daniele, P.; Galluccio, L.; Grasso, C.; Schembra, G. Service Chain Placement Optimization in 5G FANET-Based Network Edge. *IEEE Commun. Mag.* **2022**, *60*, 60–65. [[CrossRef](#)]
6. Skondras, E.; Zoumi, E.; Michalas, A.; Vergados, D.D. A network selection algorithm for supporting drone services in 5G network architectures. In Proceedings of the 2019 Wireless Telecommunications Symposium (WTS), New York, NY, USA, 9–12 April 2019; pp. 1–6.
7. Nedelea, P.L.; Popa, T.O.; Manolescu, E.; Bouros, C.; Grigorasi, G.; Andritoi, D.; Pascale, C.; Andrei, A.; Cimpoesu, D.C. Telemedicine System Applicability Using Drones in Pandemic Emergency Medical Situations. *Electronics* **2022**, *11*, 2160. [[CrossRef](#)]
8. Rajagopal, T.; Balakrishnan, A.; Valsalakumar, S.; Rajagopal, T.K.R.; Sundaram, S. Application of MSVPC-5G Multicast SDN Network Eminence Video Transmission in Drone Thermal Imaging for Solar Farm Monitoring. *Energies* **2021**, *14*, 8255. [[CrossRef](#)]
9. Santa, J.; Fernández, P.J.; Ortiz, J.; Sanchez-Iborra, R.; Skarmeta, A.F. SURROGATES: Virtual OBU to foster 5G vehicular services. *Electronics* **2019**, *8*, 117. [[CrossRef](#)]
10. Gallego-Madrid, J.; Molina-Zarca, A.; Sanchez-Iborra, R.; Bernal-Bernabe, J.; Santa, J.; Ruiz, P.M.; Skarmeta-Gómez, A.F. Enhancing extensive and remote lora deployments through mec-powered drone gateways. *Sensors* **2020**, *20*, 4109. [[CrossRef](#)]
11. Shea, C.; Hassanabadi, B.; Valaee, S. Mobility-based clustering in VANETs using affinity propagation. In Proceedings of the GLOBECOM 2009–2009 IEEE Global Telecommunications Conference, Honolulu, HI, USA, 30 November–4 December 2009; pp. 1–6.
12. Shi, L.; Jiang, Z.; Xu, S. Throughput-aware path planning for UAVs in D2D 5G networks. *Ad Hoc Netw.* **2021**, *116*, 102427. [[CrossRef](#)]
13. Jotanovic, G.; Brtko, V.; Stojanovic, J.; Stojanovic, Z.; Jausevac, G.; Dobrilovic, D. Smart City IoT On-Demand Monitoring System Using a Drone Fleet. In *International Conference on Future Access Enablers of Ubiquitous and Intelligent Infrastructures*; Springer: Berlin/Heidelberg, Germany, 2022; pp. 105–121.
14. 1609.3-2016; IEEE Standard for Wireless Access in Vehicular Environments (WAVE)–Networking Services. IEEE: Minneapolis, MN, USA, 2016.
15. 1609.2.1/D10; IEEE Draft Wireless Access in Vehicular Environments (WAVE)–Certificate Management Interfaces for End-entities. IEEE: Minneapolis, MN, USA, 2020.
16. TS 36.300 (V13.2.0); Evolved Universal Terrestrial Radio Access Network (E-UTRAN) (Rel.13). Technical Specification, 3GPP: Antipolis, France, 2016.
17. TS 124.301 (V15.8.0); LTE, 5G, Non-Access-Stratum (NAS) protocol for Evolved Packet System (EPS) (Rel.15). Technical Specification, 3GPP: Antipolis, France, 2020.
18. TS 123.501 (V15.8.0); System architecture for the 5G System (5GS) (Rel.15). Technical Specification, 3GPP: Antipolis, France, 2020.
19. IEEE Std 802.16-2017; IEEE Standard for Air Interface for Broadband Wireless Access Systems. IEEE: Minneapolis, MN, USA, 2018.
20. 802.16q-2015; IEEE Standard for Air Interface for Broadband Wireless Access Systems–Amendment 3 Multi-tier Networks. IEEE: Minneapolis, MN, USA, 2015.
21. Ahizoune, A.; Hafid, A. A new stability based clustering algorithm (SBCA) for VANETs. In Proceedings of the 37th annual IEEE conference on local computer networks-workshops, Clearwater, FL, USA, 22–25 October 2012; pp. 843–847.
22. Ren, M.; Zhang, J.; Khokhi, L.; Labiod, H.; Vèque, V. A unified framework of clustering approach in vehicular ad hoc networks. *IEEE Trans. Intell. Transp. Syst.* **2017**, *19*, 1401–1414. [[CrossRef](#)]
23. Shayea, I.; Dushi, P.; Banafaa, M.; Rashid, R.A.; Ali, S.; Sarijari, M.A.; Daradkeh, Y.I.; Mohamad, H. Handover Management for Drones in Future Mobile Networks—A Survey. *Sensors* **2022**, *22*, 6424. [[CrossRef](#)]
24. Qureshi, K.N.; Abdullah, A.H.; Bashir, F.; Iqbal, S.; Awan, K.M. Cluster-based data dissemination, cluster head formation under sparse, and dense traffic conditions for vehicular ad hoc networks. *Int. J. Commun. Syst.* **2018**, *31*, e3533. [[CrossRef](#)]
25. Aydin, Y.; Kurt, G.K.; Ozdemir, E.; Yanikomeroglu, H. Group handover for drone base stations. *IEEE Internet Things J.* **2021**, *8*, 13876–13887. [[CrossRef](#)]
26. Chen, Y.; Lin, X.; Khan, T.; Mozaffari, M. Efficient drone mobility support using reinforcement learning. In Proceedings of the 2020 IEEE Wireless Communications and Networking Conference (WCNC), Seoul, Republic of Korea, 25–28 May 2020; pp. 1–6.
27. Guidolin, F.; Pappalardo, I.; Zanella, A.; Zorzi, M. Context-aware handover policies in HetNets. *IEEE Trans. Wirel. Commun.* **2016**, *15*, 1895–1906. [[CrossRef](#)]
28. Brahim, M.B.; Mir, Z.H.; Znaidi, W.; Filali, F.; Hamdi, N. QoS-Aware Video Transmission Over Hybrid Wireless Network for Connected Vehicles. *IEEE Access* **2017**, *5*, 8313–8323. [[CrossRef](#)]

29. Zhang, L.; Ge, L.; Su, X.; Zeng, J. Fuzzy logic based vertical handover algorithm for trunking system. In Proceedings of the 2017 26th Wireless and Optical Communication Conference (WOCC), Newark, NJ, USA, 7–8 April 2017; pp. 1–5.
30. Gupta, S.; Parne, B.L.; Chaudhari, N.S. ISAG: IoT-enabled and Secrecy Aware Group-based handover scheme for e-health services in M2M communication network. *Future Gener. Comput. Syst.* **2021**, *125*, 168–187. [[CrossRef](#)]
31. Zhang, D.; Ge, H.; Zhang, T.; Cui, Y.Y.; Liu, X.; Mao, G. New multi-hop clustering algorithm for vehicular ad hoc networks. *IEEE Trans. Intell. Transp. Syst.* **2018**, *20*, 1517–1530. [[CrossRef](#)]
32. Saaty, T.L.; Vargas, L.G. The analytic network process. In *Decision Making with the Analytic Network Process*; Springer: Boston, MA, USA, 2013; pp. 1–40.
33. Saaty, T.L. *Decision Making with Dependence and Feedback: The Analytic Network Process*; RWS Publications: Pittsburgh, PA, USA, 1996.
34. Kosmopoulos, I.; Skondras, E.; Michalas, A.; Vergados, D.D. An efficient mobility management scheme for 5G network architectures. In Proceedings of the 2020 5th South-East Europe Design Automation, Computer Engineering, Computer Networks and Social Media Conference (SEEDA-CECNSM), Corfu, Greece, 25–27 September 2020; pp. 1–6.
35. Vafaei, N.; Ribeiro, R.A.; Camarinha-Matos Assessing Normalization Techniques for Simple Additive Weighting Method. *Procedia Comput. Sci. J.* **2022**, *199*, 1229–1236. [[CrossRef](#)]
36. Network Simulator 3 (NS3). Available online: <https://www.nsnam.org/> (accessed on 25 October 2022).
37. Sharma, V.; Guan, J.; Kim, J.; Kwon, S.; You, I.; Palmieri, F.; Collotta, M. MIH-SPFP: MIH-based secure cross-layer handover protocol for Fast Proxy Mobile IPv6-IoT networks. *J. Netw. Comput. Appl.* **2019**, *125*, 67–81. [[CrossRef](#)]
38. Kosmopoulos, I.; Skondras, E.; Michalas, A.; Michailidis, E.T.; Vergados, D.D. Handover Management in 5G Vehicular Networks. *Future Internet* **2022**, *14*, 87. [[CrossRef](#)]
39. Su, G.; You, P.; Yong, S. Comparative Handover Performance Analysis of MIPv6 and FMIPv6 in LEO Satellite Networks. In Proceedings of the 2017 International Conference on Network and Information Systems for Computers (ICNISC), Shanghai, China, 14–16 April 2017; pp. 30–36.
40. Degefa, F.; Ryu, J.; Kim, H.; Won, D. MES-FPMIPv6: MIH-Enabled and enhanced secure Fast Proxy Mobile IPv6 handover protocol for 5G networks *. *PLoS ONE* **2022**, *17*, e0262696. [[CrossRef](#)]
41. Wang, Y.; Wang, X.; Yi, B.; Huang, M. An efficient and reliable service customized routing mechanism based on deep learning in IPv6 network. *IET Commun.* **2022**, *16*, 2249–2264. [[CrossRef](#)]
42. Zhang, L.; Tian, Y.C. An enhanced fast handover triggering mechanism for Fast Proxy Mobile IPv6. *Wirel. Netw.* **2018**, *24*, 513–522. [[CrossRef](#)]
43. Hassan, M.M.; Tan, I.K.; Selvaretnam, B.; Poo, K.H. SINR-based conversion and prediction approach for handover performance evaluation of video communication in Proxy Mobile IPv6. *Comput. Electr. Eng.* **2019**, *74*, 164–183. [[CrossRef](#)]
44. TS 123.501 (V15.2.0); System Architecture for the 5G System (Rel.15). Technical Specification, 3GPP: Antipolis, France, 2018.
45. TS 123.203 (V12.6.0); LTE Policy and charging control architecture (Rel.12). Technical Specification, 3GPP: Antipolis, France, 2014.
46. Sahu, R.; Chaurasia, K.K.; Gupta, A.K. SINR and rate coverage of broadcast networks using stochastic geometry. In Proceedings of the 2020 International Conference on Signal Processing and Communications (SPCOM), Bangalore, India, 19–24 July 2020; pp. 1–5.
47. Yew, H.T.; Chekima, A.; Kiring, A.; Mbulwa, A.I.; Dargham, J.A.; Chung, S.K. RSS Based Vertical Handover Schemes in Heterogeneous Wireless Networks: Past, Present & Future. In Proceedings of the 2020 IEEE 2nd International Conference on Artificial Intelligence in Engineering and Technology (IICAET), Kota Kinabalu, Malaysia, 26–27 September 2020; pp. 1–5.
48. TP-Link Omada Cloud SDN Platform. Available online: <https://www.tp-link.com/us/omada-sdn/> (accessed on 29 November 2022).
49. TP-LINK EAP225 Outdoor MU-MIMO Access Point. Available online: <https://www.tp-link.com/gr/business-networking/outdoor-ap/eap225-outdoor/> (accessed on 29 November 2022).
50. Huawei RH2288H V3 Rack Server. Available online: <https://support.huawei.com/enterprise/en/intelligent-servers/rh2288h-v3-pid-9901881/> (accessed on 29 November 2022).
51. TP-LINK T2600G-28TS Jetstream Switch. Available online: <https://www.tp-link.com/gr/business-networking/managed-switch/t2600g-28ts/> (accessed on 29 November 2022).
52. TP-LINK Omada OC200 Hardware Controller. Available online: <https://www.tp-link.com/us/business-networking/omada-sdn-controller/oc200/> (accessed on 29 November 2022).
53. TP-LINK Omada Software Controller. Available online: <https://www.tp-link.com/us/support/download/omada-software-controller/> (accessed on 29 November 2022).
54. Chitanvis, R.; Ravi, N.; Zantye, T.; El-Sharkawy, M. Collision avoidance and Drone surveillance using Thread protocol in V2V and V2I communications. In Proceedings of the 2019 IEEE National Aerospace and Electronics Conference (NAECON), Dayton, OH, USA, 15–19 July 2019; pp. 406–411.